Wavelength modulation spectroscopy for measurements of gas parameters in combustion field*

Dong-Sheng Qu(屈东胜)†, Yan-Ji Hong(洪延姬), Guang-Yu Wang(王广宇), and Hu Pan(潘虎)

State Key Laboratory of Laser Propulsion & Applications, Equipment Academy, Beijing 101416, *China*

(Received 31 October 2016; revised manuscript received 15 February 2017; published online 20 April 2017)

A novel wavelength modulation spectroscopy sensor for studying gas properties near 1.4 μm is developed, validated and used in a direct-connect supersonic combustion test facility. In this sensor there are two H_2O transitions near 7185.60 cm^{-1} and 7454.45 cm^{-1} that are used to enable the measurements along the line-of-sight. According to an iterative algorithm, the gas pressure, temperature and species mole fraction can be measured simultaneously. The new sensor is used in the isolator and extender of the supersonic combustion test facility. In the isolator, the sensor resolves the transient and measured pressure, temperature and H_2O mole fraction with accuracies of 2.5%, 8.2%, and 7.2%, respectively. Due to the non-uniform characteristic in the extender, the measured results cannot precisely characterize gas properties, but they can qualitatively describe the distinctions of different zones or the changes or fluctuations of the gas parameters.

Keywords: wavelength modulation spectroscopy, sensor, gas properties, iterative algorithm

PACS: 42.68.Ca, 42.79.–e **DOI:** 10.1088/1674-1056/26/6/064207

1. Introduction

Combustion is a major source of energy,thus, it is of great significance for improving combustion efficiency and reducing combustion-generated pollutants. Understanding and optimizing the performances and processes of the combustion devices are the premise of improving the combustion performance and require a lot of diagnoses. Due to the significant advantages of non-intrusion, good temporal resolution, species selection, *in situ* measurement and robustness, tunable diode laser absorption spectroscopy (TDLAS) technology has played an increasing role in combustion research in recent decades.[1–3]

The TDLAS is an ideal tool for field testing because the technologies based on TDLAS are rugged, versatile and portable. These sensors operate by detecting species-specific absorption of narrow-band light, which is related to gas properties and can be used to measure field parameters.[4]

Wavelength modulation spectroscopy (WMS) is a representative TDLAS technique with good noise-rejection characteristics.[5] For WMS, the laser wavelength (i.e., frequency) is modulated with a high-frequency (kHz to MHz) sinusoidal signal across the absorption transition. After demodulating the detected signals, the harmonic signals can be extracted and used to infer gas parameters. Because the low-frequency is restrained after demodulation, the signal-to-noise ratio (SNR) of WMS is much more advantageous, especially for applications with small absorbance or in a high pressure environment. Also the WMS can increase the detection sensitivity and remove the effects of laser emission, fluctuation and vibration produced by the environment.[6,7] Due to these conspicuous advantages, the WMS has been widely used in many fields in the last few decades. In 1993, Philippe and Hanson developed the typical WMS which was realized by sinusoidal modulation on the injection current of a diode laser.[8] Then Li *et al.*[9] found that using the Fourier expansion and numeric integration in WMS simulation, all of the harmonic signals can be simulated. In 2007, Rieker *et al.*[10,11] realized that all the harmonics signals have the same incident intensity and detector gain. The common terms in harmonics can be eliminated by using the first-harmonics $(1f)$-normalized method which is called "calibration-free" measurement. With the maturation of the calibration-free WMS method, TDLAS sensors have been used extensively in an engine ground test facility,[12–15] coal-fired power plant,[16] and coal gasifiers.[17,18] However, when the "calibration-free" method is performed, the pressure must be known because the pressure could affect the line shape and WMS model in simulation. So the pressure deviation between simulation and experiment will induce errors in the inferred gas parameters, especially for the practical applications where the pressure may be uncertain, difficult to measure or change along the laser line-of-sight.[19]

In this paper, a new two-color WMS sensor is proposed to remove the effect of pressure and realize the measurements of gas temperature, pressure and species mole fraction in the combustion field. Also some complex phenomena in the process of supersonic combustion are revealed based on the WMS sensors. The rest of this paper is organized as follows. In Section 2, the basic theory of wavelength modulation spectroscopy is introduced and an iterative algorithm is put forward. In Section 3, we describe the experimental setup and discuss the measured results in the direct-connect supersonic

*Project supported by the Young Scientists Fund of the National Natural Science Foundation of China (Grant No. 21403299).

†Corresponding author. E-mail: hnqudongsheng@126.com

© 2017 Chinese Physical Society and IOP Publishing Ltd

combustion test facility. Finally, in Section 4, we summarize the analyses and draw some conclusions.

2. Theory

2.1. Wavelength modulation spectroscopy

The absorption of a monochromatic light beam at frequency v through a uniform gas medium can be described by Beer–Lambert law

$$\tau_v = \left(\frac{I_t}{I_0}\right)_v = \exp\left(-\alpha_v\right), \tag{1}$$

where τ_v is the transmission coefficient; I_t and I_0 are the transmitted and incident beam intensity, respectively; α_v represents the spectral absorbance at optical frequency v and is related to specific gas property

$$\alpha_v = PXS(T)\phi_v L, \tag{2}$$

where P (in unit atm, 1 atm = 1.01325×10^5 Pa) is the total gas pressure, X is the mole fraction of absorbing species, $S(T)$ (in units $\mathrm{cm^{-2}\cdot atm^{-1}}$) is the line-strength, ϕ_v (in unit cm) is the line-shape function, and L (in unit cm) is the optical path length. The temperature-dependent line-strength is given by

$$\begin{aligned} S(T) &= S(T_0)\frac{Q(T_0)}{Q(T)}\left(\frac{T_0}{T}\right)\exp\left[-\frac{hcE''}{k}\left(\frac{1}{T}-\frac{1}{T_0}\right)\right] \\ &\times\left[1-\exp\left(\frac{-hcv_0}{kT}\right)\right]\left[1-\exp\left(\frac{-hcv_0}{kT_0}\right)\right]^{-1}, \end{aligned} \tag{3}$$

where T_0 is the reference temperature (typically 296 K), $S(T_0)$ is the line-strength at T_0, $Q(T)$ is the partition function of the absorbing molecule, k (in units $\mathrm{J\cdot K^{-1}}$) is the Boltzmann's constant, h (in units J·s) is the Planck's constant, E'' (in unit $\mathrm{cm^{-1}}$) is the lower-state energy, c (in units $\mathrm{cm\cdot s^{-1}}$) is light speed, and ν_0 (in unit $\mathrm{cm^{-1}}$) is the line-center frequency of the transition.

In most of the applications, line-shape function ϕ_v is modeled by the Voigt profile which is the convolution of the Gaussian and Lorentzian profiles. The ϕ_v can be written as

$$\phi(v) = \frac{\sqrt{\ln 2}}{\pi^{3/2}}\frac{\Delta v_c}{\Delta v_D}\int_{-\infty}^{+\infty}\frac{\exp\left[-\ln 2\cdot(t-v_0)^2/\Delta v_D^2\right]}{\Delta v_c^2+(v-t)^2}\mathrm{d}t, \tag{4}$$

where Δv_c and Δv_D are the line widths of Lorentzian and Gaussian profiles and can be expressed as

$$\begin{cases} \Delta v_D = v_0\sqrt{\dfrac{8kT\ln 2}{mc^2}} = 3.581\times10^{-7}v_0\sqrt{\dfrac{T}{M}}, \\ \Delta v_c = P\sum\limits_j\left(X_j\cdot\gamma_j(T_0)\cdot\left(\dfrac{T_0}{T}\right)^{n_j}\right), \end{cases} \tag{5}$$

where M (in units $\mathrm{g\cdot mol^{-1}}$) is the molecular weight of the absorbing molecule, $\gamma_j(T_0)$ (in units $\mathrm{cm^{-1}\cdot atm^{-1}}$) is the broadening coefficient at reference temperature, and n_j is the temperature exponent.

Δv_D is a function of temperature and Δv_c depends on gas composition and collisional coefficient. In the combustion diagnosis, it is common to only consider the self-broadening (collisions take place between absorbing species and absorbing species) and air-species broadening (collisions take place between absorbing species and air). Then the Δv_c can be expressed as

$$\begin{aligned} \Delta v_c &= P\cdot X\cdot\gamma_{self}(T_0)\cdot\left(\frac{T_0}{T}\right)^{n_{self}} \\ &+P\cdot(1-X)\cdot\gamma_{air}(T_0)\cdot\left(\frac{T_0}{T}\right)^{n_{air}}, \end{aligned} \tag{6}$$

where $\gamma_{self}(T_0)$ (in units $\mathrm{cm^{-1}\cdot atm^{-1}}$) and $\gamma_{air}(T_0)$ (in units $\mathrm{cm^{-1}\cdot atm^{-1}}$) are the self-broadening coefficient and air-broadening coefficient of the transition of absorbing species, n_{self} and n_{air} are the corresponding temperature exponents.

The line-center frequency ν_0, line-strength $S(T_0)$, lower-state energy E'', broadening coefficient $\gamma_j(T_0)$ and temperature exponent n_j are the spectroscopic parameters of the transition and can be found in the HITRAN database[20] or measured.[21]

Since the line-shape function ϕ_v is normalized in the frequency domain, so the integrated absorbance A of transition can be given by

$$A = \int_{-\infty}^{\infty}\alpha_v\mathrm{d}v = PXS(T)L. \tag{7}$$

Wavelength modulation spectroscopy (WMS) is a relatively complex technique. For WMS, the laser injection current is sinusoidally modulated rapidly, producing modulations in laser wavelength or frequency and intensity. The laser frequency $v(t)$ can be expressed as

$$v(t) = \bar{v} + a\cos(2\pi ft), \tag{8}$$

where $\bar{v}$ is the center laser frequency, a (in unit $\mathrm{cm^{-1}}$) is the modulation depth, and f (in unit Hz) is the modulation frequency. The corresponding intensity modulation $I_0(t)$ is represented by

$$I_0(t) = \overline{I_0}(t)\left[1+i_0\cos(2\pi ft+\psi_1)+i_2\cos(2\pi ft+\psi_2)\right], \tag{9}$$

where $\overline{I_0}(t)$ is the center laser intensity, i_0 and i_2 are the linear and nonlinear intensity modulation amplitude with corresponding phase shifts ψ_1 and ψ_2 between intensity and frequency modulation. The laser frequency $v(t)$ and intensity modulation $I_0(t)$ are related to the laser source and must be measured in the laboratory. After obtaining the laser frequency $v(t)$ and intensity modulation $I_0(t)$, the transmitted laser intensity can be simulated from the Beer–Lambert law

$$\begin{aligned} I_t(t) &= I_0(t)\cdot\tau = I_0(t)\cdot\exp(-\alpha_v) \\ &= I_0(t)\cdot\exp(-A\cdot\phi_v). \end{aligned} \tag{10}$$

Then using the lock-in amplifier, the harmonics signals (nf) can be simulated. The detailed procedure for simulation is

shown in Fig. 1. The main simulation process is 1) measure the laser frequency $v(t)$ and incident laser intensity $I_0(t)$ which is in the absence of the absorbing species simultaneously; 2) calculate the integrated absorbance A, line widths Δv_c and Δv_D of the transition by using the spectroscopic parameters and gas parameters (i.e., gas temperature, pressure, and mole fraction); 3) simulate the absorbance spectrum $\alpha(v)$ near the transition; 4) convert the absorbance spectrum from the frequency domain to the time domain by using the laser frequency $v(t)$ and obtain the absorbance spectrum time-history $\alpha(t)$; 5) simulate the time-history of laser transmitted intensity $I_t(t)$ by using the intensity modulation $I_0(t)$ and Beer-Lambert law; 6) extract the WMS-nf signals from the simulated $I_t(t)$ by using the lock-in amplifier.

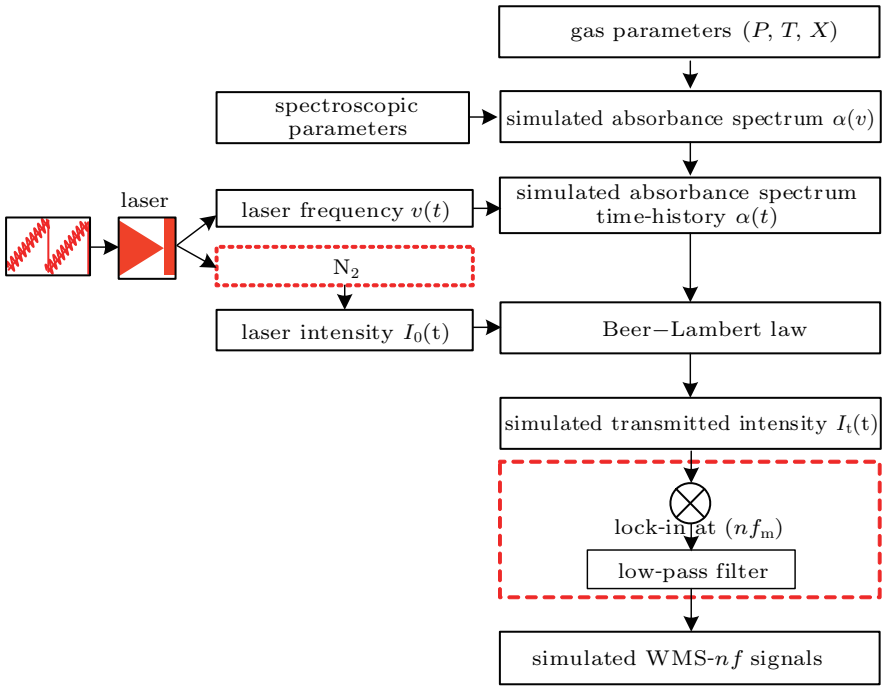


Fig. 1. (color online) Detailed procedure for simulation of harmonic signals.

The harmonic signals are related to gas temperature, pressure, and mole fraction. Using the simulated and measured harmonic signals, the quantitative relationship between harmonic signal and gas property can be established. Then the quantitative measurements of gas parameters in the unknown condition can be realized and the calibration-free can be achieved.

2.2. Measurement methods of gas parameters

In the method presented here it is assumed that the gas pressure and temperature, and absorbing species mole fraction are unknown, which is typical of the case of practical application. In this method, the harmonic signals from two transitions can be used to infer unknown gas parameters. The harmonic signals each are a function of temperature, pressure, and mole fraction. However, the different harmonic signals are the sensitivity functions of different gas parameters. From the numerical simulation and experimental measurement, it is found that the $2f/1f$ peak ratio of two transitions approximates a function of temperature which is shown in Fig. 2.

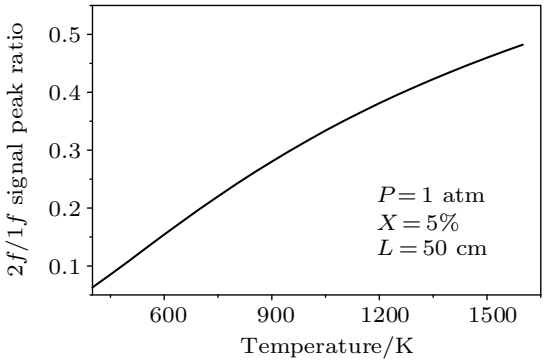


Fig. 2. Simulated $2f/1f$ peak ratio (7454.45 cm^{-1} and 7185.60 cm^{-1}) as a function of temperature.

The $2f/1f$ peak of one transition asa function of mole fraction is shown in Fig. 3(a), and the ratio between $4f$ peak and $2f$ peak ($4f_{peak}/2f_{peak}$) of one transition versus pressure is shown in Fig. 3(b). The trend shows that the $2f/1f$ peak of one transition is a monotonically increasing function of mole fraction. However, the $4f_{peak}/2f_{peak}$ is a monotonically decreasing function of pressure.

So in order to realize the measurements of gas temperature, pressure and mole fraction simultaneously, the $2f/1f$, $2f$, and $4f$ signals of two transitions need to be used. Here an iterative algorithm is put forward to measure the gas parameters by using the $2f/1f$, $2f$, and $4f$ signals of two transitions. The flow chart of the iterative process is shown in Fig. 4.

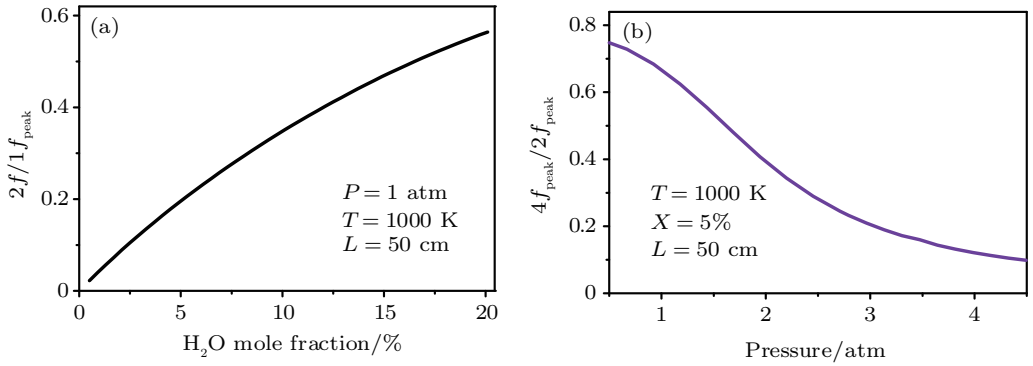


Fig. 3. (color online) (a) Simulated $2f/1f$ peak of one transition (7185.60 cm^{-1}) as a function of mole fraction; (b) simulated $4f_{peak}/2f_{peak}$ of one transition (7185.60 cm^{-1}) as a function of pressure.

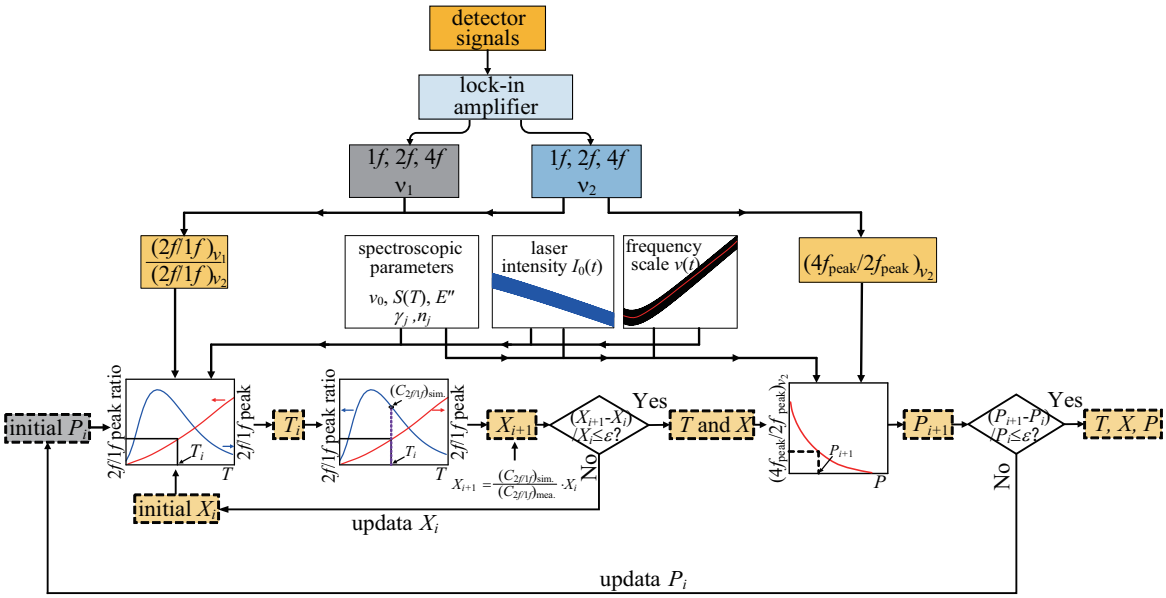


Fig. 4. (color online) Flow chart of iterative process based on wavelength modulation spectroscopy.

The basic steps are listed as follows.

(i) Extract the measured harmonic signals ($2f/1f$, $2f$, $4f$) of two transitions from the measured detector signals by using the lock-in amplifier.

(ii) Estimate measured field and guess the initial pressure (P_i) and mole fraction (X_i).

(iii) Simulate the relation curves of $2f/1f$ peak ratio of two transitions and $2f/1f$ peak of one transition as a function of temperature at the same time.

(iv) Get the temperature (T_i) after comparing the measured $2f/1f$ peak ratio with the simulated curve.

(v) Get the $2f/1f$ peak of one transition at T_i and calculate the new mole fraction (X_{i+1}) by using the equation

$$X_{i+1} = \frac{(C_{2f/1f})_{\text{meas.}}}{(C_{2f/1f})_{\text{sim.}}} X_i, \tag{11}$$

where $(C_{2f/1f})_{\text{meas.}}$ is the measured $2f/1f$ peak and $(C_{2f/1f})_{sim.}$ is the simulated $2f/1f$ peak.

(vi) Update the X_i and repeat Steps 2–6 until the condition ($|X_{i+1} - X_i|/X_i \leq \varepsilon$) is met.

(vii) Simulate the relation curve of $4f_{\text{peak}}/2f_{\text{peak}}$ of one transition as a function of pressure by using the calculated temperature and mole fraction.

(viii) Get the pressure (P_i) after comparing the measured $4f_{\text{peak}}/2f_{\text{peak}}$ with simulated curve.

(ix) Update the P_i and repeat Steps 2–8 until the condition ($|P_{i+1} - P_i|/P_i \leq \varepsilon$) is met.

(x) Obtain the pressure, temperature and mole fraction.

3. Experimental method and sensor validation

3.1. Selection of transitions

Selecting an appropriate target molecule and transitions was critical to the success in all laser absorption sensors. H_2O vapor was an especially attractive target molecule for the current sensor due to its presence in the most combustion-driven flows. In the near-infrared spectrum range, there were several thousands of H_2O vapor transitions and it was easy to choose appropriate pairs of H_2O transitions which have moderate line-strength and good temperature sensitivity. Using the wave-

length modulation spectroscopy sensor, two H_2O transitions near 7185.60 cm^{-1} and 7454.45 cm^{-1} were selected to measure the field parameters. It should be noted that although the selected H_2O vapor transitions may not be the optimal choices, the two transitions were widely used and accessed by the distributed feedback diode (DFB) lasers available in our group. The characteristics of the selected H_2O transitions are listed in Table 1.

Figure 5 plots the line-strength of two H_2O transitions and their ratio each as a function of temperature. As shown in Fig. 5, the trend that the line-strength of two H_2O transitions varying as a function of temperature shows an obvious discrepancy. However, the line-strength ratio of two H_2O transitions is a monotonic function of temperature.

Table 1. Characteristics of the selected H_2O vapor transitions.

v_0/cm^{-1}	E''/cm^{-1}	$S(T_0)/(cm^{-2}\cdot atm^{-1})$	$\gamma_{air}/(cm^{-1}\cdot atm^{-1})$	n_{air}	$\gamma_{self}/(cm^{-1}\cdot atm^{-1})$	n_{self}
7185.60	1045.06	1.88×10^{-2}	0.041	0.65	0.205	0.59
7454.45	1962.51	1.73×10^{-4}	0.0323	0.37	0.198	0.56

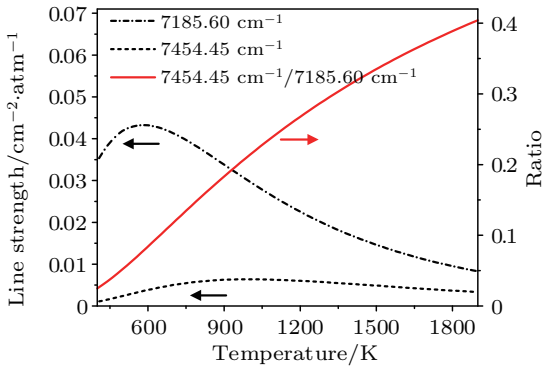


Fig. 5. (color online) Line-strengths of line 7454.45 cm^{-1} and 7185.60 cm^{-1} and their ratio versus temperature.

3.2. Facility description of supersonic combustion

Tests were performed in the direct-connect supersonic combustion test facility, shown in Fig. 6. The facility was oriented vertically, with the isolator, combustor and extender above floor level. The combustion heater was below ground and the method of producing high enthalpy flows was by combustion-heating the H_2-air, then expanding through a supersonic nozzle with oxygen replenishment. During testing, a Mach 2.5 nozzle was used to simulate hypersonic flight condition where the total pressure was 10atm and total temperature was 1252K. The nozzle was directly attached to the isolator whose section was 70 mm×51 mm. The isolator was followed by the fuel injection block and combustor where there is approximately 8-cm upstream of fuel injection and its flow path diverged along the injector-side wall at an angle of 1.3°. Heated ethylene was injected through five ports of the combustor with a 20-cm-long upstream of the leading edge of a cavity flame holder. The divergence continued all the way to the extender whose inset section was 70 mm×82.6 mm and outset section was 70 mm×107 mm in size. The test facility was outfitted with some pressure transducers in order that the system can be monitored.

In order to realize the optical measurement in the facility, six slot windows on the isolator and extender were designed which can allow optical access across the flow. The length of isolator was 314 mm and there were two slot windows on the wall which were 137 mm and 177 mm from the top of the isolator, respectively. As shown in Fig. 6, four separate sets of windows on the extender which could offer optical access were 230 cm away from the top of the combustor.

During the several seconds of facility operation, combustion tests were conducted with C_2H_4 fuel at a fuel-air equivalence ratio of 0.3580. Ethylene was injected into the mixture from instream injectors centered in the holes located in a baffle plate of the combustor section. Ignition of the gas mixture was achieved using an electric-spark-active torch ignitor.

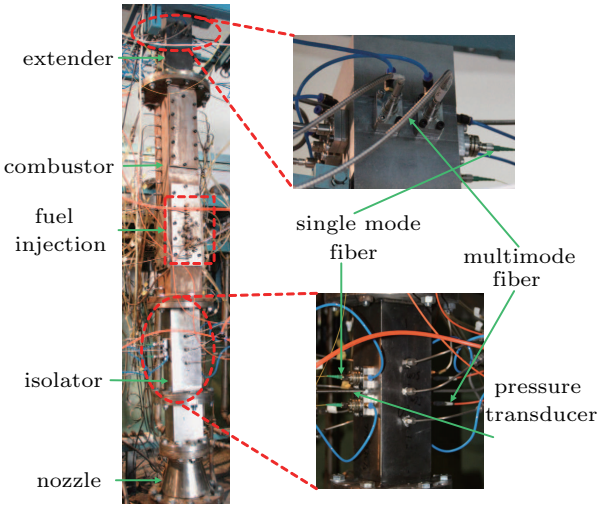


Fig. 6. (color online) Photos of direct-connect supersonic combustion test facility with six TDLAS measurement locations.

3.3. TDLAS sensor

A diagram view of the optical setup and TDLAS hardware used in the sensor is shown in Fig. 7. The computer with data acquisition cards (National Instruments, PCI-6115), DFB Lasers (NEL, NLK1B5EAAA), laser controller (ILX Lightwave, LDC-3900), fiber combiner/splitters (OZ Optics), InGaAs (EOS IGA-030-E5/4 MHz) detectors were all located in the control room. Two fiber-coupled lasers near 1391.7 nm and 1343.3 nm were used to probe H_2O vapor transitions (7185.60 cm^{-1} and 7454.45 cm^{-1}). Both

lasers were independently controlled by adjusting injection current and temperature via an ILX LDC power source. Two lasers were both set with a constant bias injection current of about 70 mA. After tuning the laser temperature (22.8° and 26.8°), the wavelengths near the selected absorption features (7185.60 $cm^{-1}$and 7454.45 cm^{-1}) were obtained.

The light beams from the two lasers were combined into a 9-μm core single-mode fiber, and the combined signal was split into six separate single-mode fibers. The fibers were routed through the blast wall into the test cell and were connected to six pitch lenses (Thorlabs, F240APC-C) on the test facility. As shown in Fig. 7, the measurement LOSs in the isolator were numbered "LOS 1" and "LOS 2". In the extender, four separate sets of windows which could offer optical access were numbered "LOS 3", "LOS 4", "LOS 5", and "LOS 6". The beam was transmitted across the test region and the larger collimator (Oz Optics, HPUCO-25-1300-M-10BQ) was used to focus the free space beam into the 400-μm core multi-mode fiber. The multi-mode fiber routes the collected signal across the wall into the detector. Through long BNC cables, the detector signal was back to the computer for a data acquisition system. The regions behind the window and the slots were purged with N_2 to remove interfering absorption by H_2O vapor in the air.

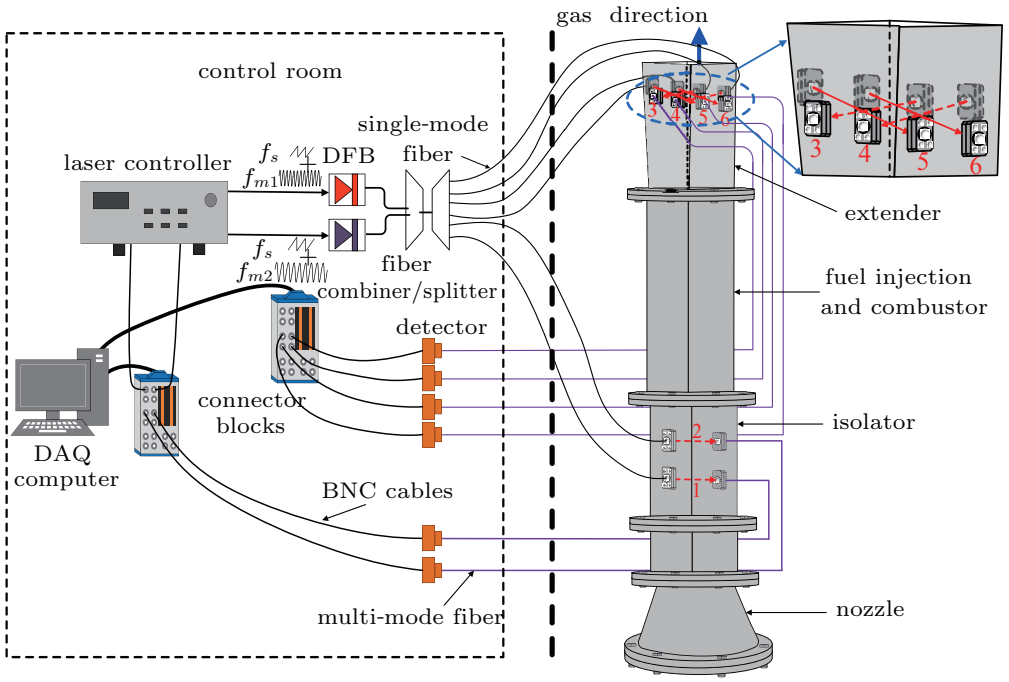


Fig. 7. (color online) Schematic diagram of optical setup and TDLAS sensor hardware in measurements conducted at the test facility.

3.4. Results and discussion

For WMS measurements, frequency division multiplexing technology is adopted to realize the measurement. Each laser is injection current modulated with a scanning sawtooth at 1 kHz. The laser near 1391.7 nm was modulated at 280 kHz with the modulation depth $a = 0.07$ cm^{-1} and the laser near 1343.3 nm was modulated at 240 kHz with the modulation depth $a = 0.10$ cm^{-1}. It should be noted that the incident laser intensity should be measured in the absence of the absorbing species. Therefore, the incident laser intensity is measured before the test when the laser path is purified with nitrogen, which can eliminate the interference absorption by H_2O vapor. The incident laser intensity and etalon signal are acquired synchronously. Because the intensity and wavelength response to injection current are close to linearity for DFB laser, the sum of polynomial and sinusoid is employed to fit frequency signals $v(t)$. Having the intensity and frequency signals, the WMS-nf signals could be simulated as shown in Fig. 1.

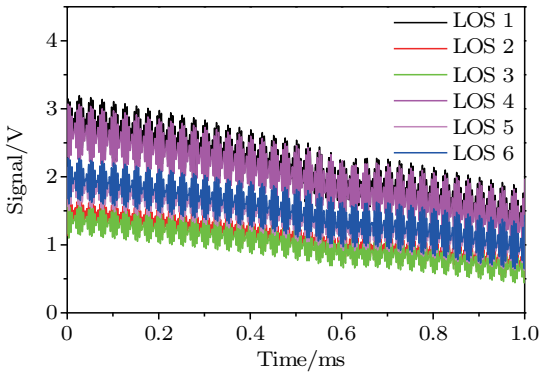


Fig. 8. (color online) Measured transmitted laser intensities during the test.

During the test, the time-resolved absorption data of six InGaAs photodiodes are simultaneously collected by the data acquisition cards with 5 MS/s. As shown in Fig. 8, although the detector signals have the different laser intensities due

to the emission, non-absorbing transmission or detector gain. However, it should be noted that all harmonic components are proportional to laser intensity while the transmission only depends on gas absorption property. Taking the ratio between two harmonic signals would eliminate the effects of laser intensity.

3.4.1. Measurement in the isolator

The detector signals are input to a digital lock-in amplifier which can isolate the harmonics at the frequencies of interest, namely $1f$, $2f$, and $4f$. The harmonic signal could be expressed in the complex form as $S = X + \mathrm{i}Y$. Using the phase-insensitive lock-in, the X component (transmitted signal intensity $\times \cos(n \cdot 2\pi ft)$) and Y component (transmitted signal intensity $\times \sin(n \cdot 2\pi ft)$) are produced. Then a 20-kHz Butterworth filter is used to separate the X component from the Y component of harmonic signals. The magnitude of WMS-nf signal can be written as

$$S_{nf} = \sqrt{X_{nf}^2 + Y_{nf}^2}. \tag{12}$$

Figure 9 shows the measured WMS-nf signals for a single-scan measurement of the H_2O transitions near 7185.60 cm^{-1} and 7454.45 cm^{-1}. Having obtained the simulated and measured harmonic signals ($1f$, $2f$, and $4f$), calibration-free WMS could be used to infer gas temperature, H_2O mole fraction and pressure.

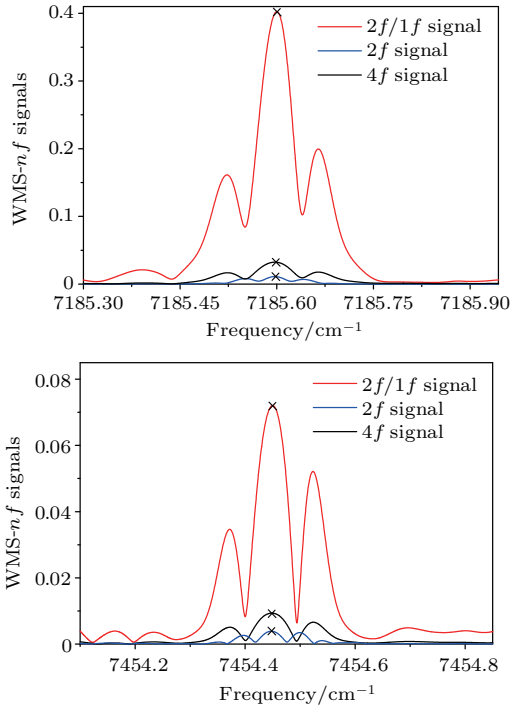


Fig. 9. (color online) Measured harmonic signals of the H_2O transitions near 7185.60 cm^{-1} and 7454.45 cm^{-1} within a scanning period.

During the testing of the TDLAS sensor, the Mach 2.5 nozzle is used to produce the nominal test condition. The gas properties in the isolator could be computed using the facility-supplied one-dimensional (1D) thermodynamic equilibrium. The predicted values of static temperature, static pressure, and water mole fraction are 647 K, 0.569 atm, and 0.148, respectively.

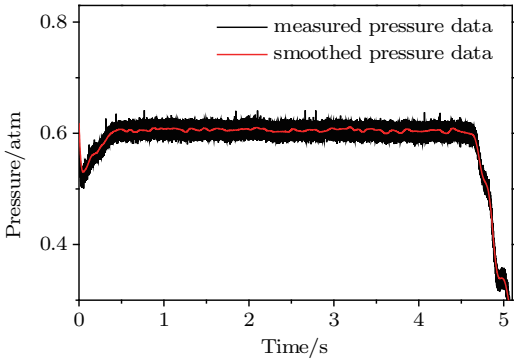


Fig. 10. (color online) Plot of pressure versus time, measured by pressure transducer.

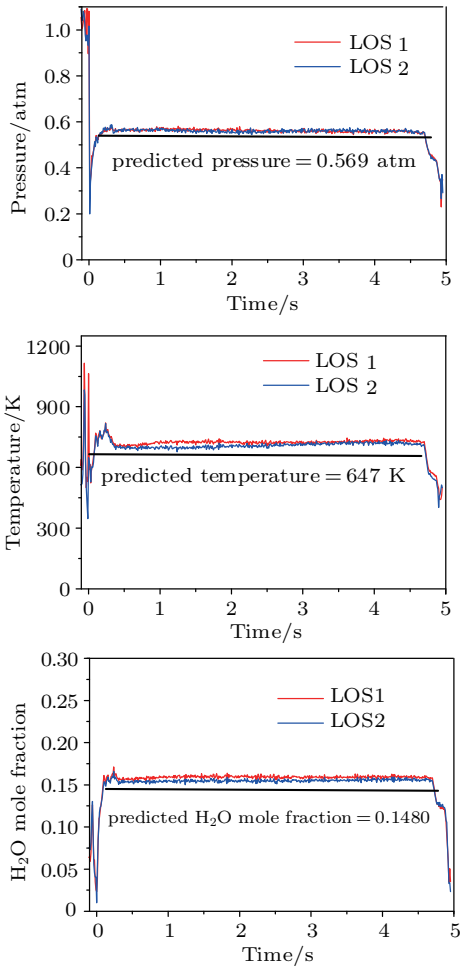


Fig. 11. (color online) Plots of measured pressure, temperature, and H_2O mole fraction versus time in the isolator.

In order to monitor the stability of the field, a pressure transducer is mounted at the wall surface of the isolator. Figure 10 shows the plot of pressure versus time of 5 s obtained from the test. As shown in Fig. 10, the time-dependent pressure shows very small deviation from that under the stable condition. The red curve shows the data after it has been smoothed to help display the imperceptible changes of the data.

Using the iterative algorithm (Subsection 2.2), the measured gas temperature, H_2O mole fraction and pressure for LOS 1 and LOS 2 are shown in Fig. 11. From Fig. 11, it follows that the difference in measured result between LOS 1 and LOS 2 is negligibly small because the flow in the isolator has a good uniformity. Compared with the predicted values, the most relative errors of pressure, temperature and H_2O mole fraction are less than 2.5%, 8.2%, and 7.2%. So it is proved that the TDLAS sensor can be suitable for the uniform environment.

3.4.2. Measurement in the extender

The TDLAS technology is the line-of-sight measurement and can describe the gas properties in the uniform environment. However, when the facility is operated with combustion, flow through the extender becomes non-uniform.

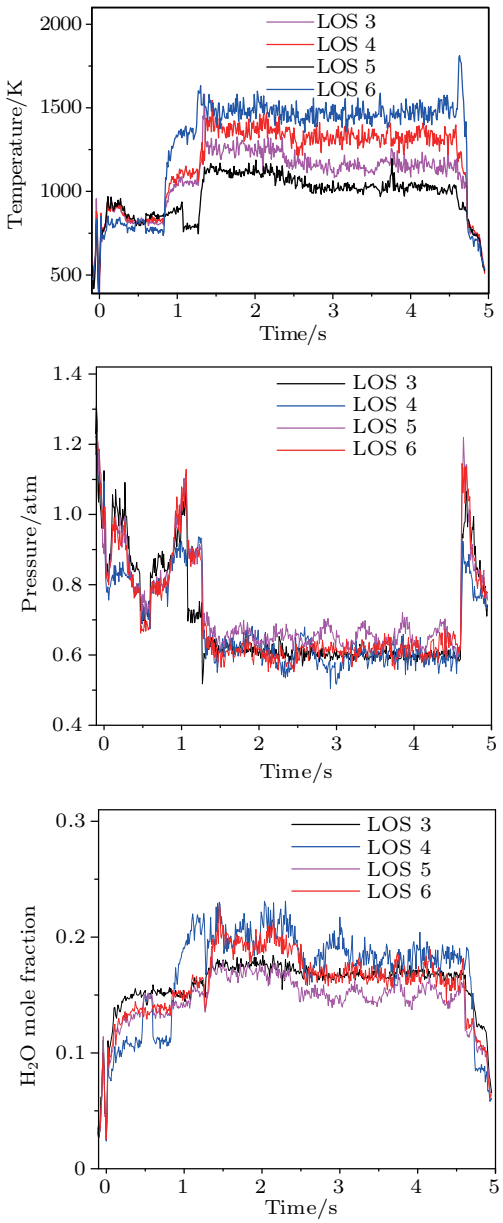


Fig. 12. (color online) Plots of measured temperature, pressure, and H_2O mole fraction versus time from LOS 3, LOS 4, LOS 5, and LOS 6.

If we suppose the flow in the extender is uniform, we can also obtain the temperature, pressure, and H_2O mole fraction by using the iterative algorithm. Due to the non-uniform characteristics of LOS in the extender, the measured temperature, pressure, and H_2O mole fraction in the extender by using this method cannot be used to quantitatively describe the flow. However, the measured results based on TDLAS in the non-uniform field can qualitatively describe the change of field. Figure 12 shows the measured results from LOS 3, LOS 4, LOS 5, and LOS 6. As shown in Fig. 12, after 0.5 s from ignition time using an electric-spark-active torch ignitor, the measured results tend towards stability but the fluctuations exceed the results in the isolator.

Also what can be seen is that the temperature of LOS 6 is the highest and the result of LOS 5 is lowest. This is because the LOS 6 is close to the wall along the fuel-injector while the LOS 5 is near the wall opposite to the fuel-injector.

It should also be noted that the multi-beam results based on TDLAS could be used to distinguish the differences in field characteristic. The sectional views from LOS 3, LOS 4, LOS 5, and LOS 6 are shown in Fig. 13. The right half is the high temperature zone and the left half is the low temperature zone from the measured temperature of LOS 5 and LOS 6. This is because the fuel-injector is mounted on the right wall. It is not hard to understand that the measured values of LOS 3 and LOS 4 lie in the middle between LOS 5 and LOS 6.

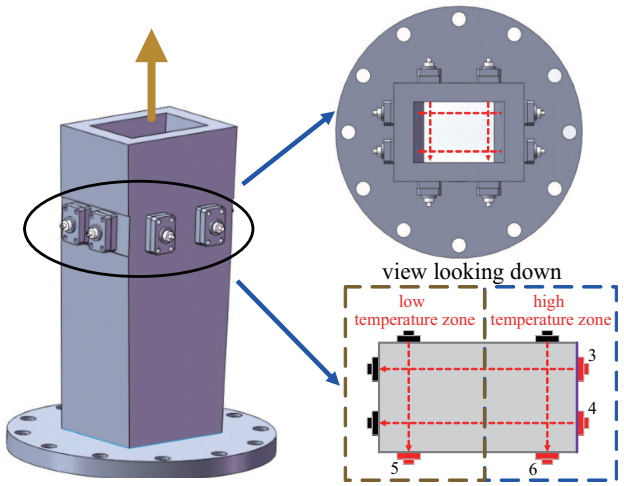


Fig. 13. (color online) Sectional views from LOS 3, LOS 4, LOS 5, and LOS 6.

It is worth pointing out that during the run of the test, the sensor is used in harsh environments such as high temperature, high velocity and strong vibration, and the sensor has a good adaptability.

4. Conclusions

The design and use of a sensor based on TDLs determining pressure, temperature and H_2O mole fraction are presented

in a direct-connect scramjet fueled by ethylene. Based on simulation and experiment, an iterative algorithm is built to infer gas parameters from $2f/1f$ and $4f_{\rm peak}/2f_{\rm peak}$ signals of two H_2O transitions. The gas flow in the isolator of direct-connect supersonic combustion test facility has a good uniformity, the results measured by using the iterative algorithm are in good agreement with the predicted values. The most relative errors of pressure, temperature and H_2O mole fraction are less than 2.5%, 8.2%, and 7.2%, respectively. After the combustion test, the flow in the extender is non-uniform, the results measured by using the sensor cannot quantitatively characterize gas parameters. However, the results can qualitatively describe the distinctions of different zones or the changes and fluctuations of the gas parameters.

References

[1] Hodgkinson J and Ralph P T 2013 *Meas. Sci. Technol.* **24** 012004
[2] Bolshov M A, Kuritsyn Y A and Romanovskii 2015 *Spectrochimica Acta B* **106** 45
[3] Krishna Y and O'Byrne Sean 2016 *J. Indian I Sci.* **96** 18
[4] Hanson R K 2011 *Proc. Combust. Inst.* **33** 1
[5] Goldenstein C S, Jeffries J B and Hanson R K 2013 *J. Quantum Spectrosc. Radiat. Transfer* **130** 100
[6] Sun K, Sur R, Chao X, Jeffries J B, Hanson R K, Pummill R J and Whitty K J 2013 *Proc. Combust. Inst.* **34** 3593
[7] Jatana G S, Magee M, Fain D, Naik SV, Shaver G M and Lucht R P 2015 *Appl. Opt.* **54** 1220
[8] Philippe L C and Hanson R K 1993 *Appl. Opt.* **32** 6090
[9] Li H J, Rieker G B, Liu X, Jeffries J B and Hanson R K 2006 *Appl. Opt.* **45** 1052
[10] Rieker G B, Jeffries J B and Hanson R K 2009 *Appl. Opt.* **48** 5546
[11] Rieker G B, Jeffries J B, Hanson R K, Mathur T, Gruber M R and Carter C D 2009 *Proc. Combust. Inst.* **32** 831
[12] Goldenstein C S, Spearrin R M, Jeffries J B and Hanson R K 2015 *Proc. Combust. Inst.* **35** 3739
[13] Schultz I A, Goldenstein C S, Spearrin R M, Jeffries J B and Hanson R K 2014 *J. Propul. Power* **30** 1595
[14] Goldenstein C S, Schultz I A, Spearrin R M, Jeffries J B and Hanson R K 2014 *Appl. Phys. B* **116** 717
[15] Goldenstein C S, Almdovar C A, Jeffries J B, Hanson R K and Brophy C M 2014 *Meas. Sci. Technol.* **25** 105104
[16] Chao X, Jeffries J B and Hanson R K 2013 *Proc. Combust. Inst.* **34** 3583
[17] Sur R, Sun K, Jeffries J B, Socha J G and Hanson R K 2015 *Fuel* **150** 102
[18] Sur R, Sun K, Jeffries J B and Hanson R K 2014 *Appl. Phys. B* **115** 9
[19] Che L, Ding Y J, Peng Z M and Li X H 2012 *Chin. Phys. Lett.* **29** 067801
[20] Rothmana L S, Gordon I E, Babikov Y, *et al.* 2013 *J. Quantum Spectrosc. Radiat. Transfer* **130** 4
[21] Goldenstein C S, Jeffries J B and Hanson R K 2013 *J. Quantum Spectrosc. Radiat. Transfer* **130** 100